

CrystEngComm

Accepted Manuscript



This is an *Accepted Manuscript*, which has been through the Royal Society of Chemistry peer review process and has been accepted for publication.

Accepted Manuscripts are published online shortly after acceptance, before technical editing, formatting and proof reading. Using this free service, authors can make their results available to the community, in citable form, before we publish the edited article. We will replace this *Accepted Manuscript* with the edited and formatted *Advance Article* as soon as it is available.

You can find more information about *Accepted Manuscripts* in the [Information for Authors](#).

Please note that technical editing may introduce minor changes to the text and/or graphics, which may alter content. The journal's standard [Terms & Conditions](#) and the [Ethical guidelines](#) still apply. In no event shall the Royal Society of Chemistry be held responsible for any errors or omissions in this *Accepted Manuscript* or any consequences arising from the use of any information it contains.

Elastic properties and acoustic dissipation associated with a disorder-order ferroelectric transition in a metal-organic framework

Zhiying Zhang^{a,b,*}, Wei Li^{c,*}, Michael A. Carpenter^b, Christopher J. Howard^d, Anthony K. Cheetham^c

^a*Department of Metallic Materials, School of Materials Science and Engineering, Wuhan University of Technology, 122 Luoshi Road, Wuhan, Hubei, 430070, China*

^b*Department of Earth Sciences, University of Cambridge, Downing Street, Cambridge, CB2 3EQ, United Kingdom*

^c*Department of Materials Science and Metallurgy, University of Cambridge, 27 Charles Babbage Road, Cambridge, CB3 0FS, United Kingdom*

^d*School of Engineering, University of Newcastle, New South Wales, 2308, Australia*

*To whom correspondence should be addressed. E-mail: zhiyingzhang@whut.edu.cn, w1276@cam.ac.uk

Abstract

Elastic properties and acoustic dissipation associated with the disorder-order ferroelectric transition in a single crystal metal-organic framework (MOF), $[\text{NH}_4][\text{Zn}(\text{HCOO})_3]$, have been investigated using resonant ultrasound spectroscopy (RUS) in the temperature range between 10 K and 300 K. The paraelectric to ferroelectric transition at around 192 K is triggered by the disorder-order transition of ammonium cations within the structure and changes of hydrogen bonding, accompanied by a structural phase transition from the non-

polar hexagonal space group $P6_322$ to the polar hexagonal space group $P6_3$. The elastic moduli, which are proportional to the square of resonant frequencies, gradually decrease with increasing temperature, and the rate of decrease changes markedly near the transition temperature. The acoustic dissipation tends to gradually increase with increasing temperature, but with a peak near the transition point. This pattern of behaviour can be understood by analogy with phase transitions driven by hydrogen bonding coupled to lattice strain in the mineral lawsonite $[\text{CaAl}_2\text{Si}_2\text{O}_7(\text{OH})_2 \cdot \text{H}_2\text{O}]$. The newly formed hydrogen bonds act as braces to stiffen the structure, as opposed to the elastic softening which typically occurs at displacive phase transitions. The acoustic loss mechanism involves dynamical disordering of hydrogen atoms between symmetry related positions and coupling of their motion with local lattice strain.

1. Introduction

Metal-organic frameworks (MOFs) are hot topics due to their hybrid inorganic-organic nature, diverse and tuneable properties, and potential applications in catalysis, gas storage and separation, magnetism and ferroelectricity.¹ Multiferroic MOFs with at least two ordered forms among ferroelasticity, ferroelectricity, and ferromagnetism are of particular interest, and a few MOFs have been studied using X-ray diffraction (XRD), differential scanning calorimetry (DSC), magnetic and dielectric measurements.² Elastic and anelastic properties of MOFs have been investigated by nanoindentation, atomic force microscopy (AFM), Brillouin scattering (BS), resonant ultrasound spectroscopy (RUS) and computer simulation.³ In the MOF family of $[(\text{CH}_3)_2\text{NH}_2][\text{M}(\text{HCOO})_3]$ ($\text{M} = \text{Fe}, \text{Co}, \text{Ni}, \text{Mn}$) with perovskite-like structures, paraelectric–ferroelectric phase transitions occur between 160 K and 185 K (Fe: 160 K; Co: 165 K; Ni: 180 K, Mn: 185 K), which are triggered by order-disorder of the alkylammonium cations located in the framework cavities, and a spin-canted

antiferromagnetic ordering transition can occur below 40 K arising from the metal ions within the framework skeletons.^{2a, 3e, 4} In the MOF family of $[\text{NH}_4][\text{M}(\text{HCOO})_3]$ ($\text{M} = \text{Mn}, \text{Fe}, \text{Co}, \text{Ni}, \text{Zn}, \text{Mg}$), paraelectric to ferroelectric phase transitions accompanied by a structural phase transition from the non-polar hexagonal space group $P6_322$ to the polar hexagonal space group $P6_3$ occur between 191 and 255 K (Co: 191 K; Zn: 192 K; Ni: 199 K; Fe: 212 K; Mn: 254 K, Mg: 255 K).^{3h, 5} These are triggered by disorder–order transitions of the ammonium cations and their displacement within the framework channels. Weak magnetic ordering (spin-canted antiferromagnetic ordering for the Mn, Co and Ni members, and ferromagnetic ordering for the Fe member) occurs between 8 K and 30 K for the magnetic members (Mn: 8.4 K; Fe: 9.4 K; Co: 9.8 K; Ni: 29.5 K) based on studies by single-crystal XRD, DSC, magnetic and dielectric measurements.^{3h, 5} The focus of this work is to investigate the elastic properties and acoustic dissipation related to phase transitions in $[\text{NH}_4][\text{Zn}(\text{HCOO})_3]$ using RUS, which is a powerful tool for characterising strain relaxation effects associated with ferroelectric and magnetic transitions but is rarely used in studies of MOFs.^{3e, 3f}

2. Experimental Details

2.1. Materials synthesis

Single-crystals of $[\text{NH}_4][\text{Zn}(\text{HCOO})_3]$ (**1**) were prepared according to the method described elsewhere in the literature.^{5b} A 5 ml methanol solution of 0.4 M HCOOH and 0.8 M HCOONH₄ was placed at the bottom of a glass tube, then 2 ml of methanol was added, followed by carefully layering of a 5 ml methanol solution of 0.10 M $\text{Zn}(\text{ClO}_4)_2 \cdot 6\text{H}_2\text{O}$. Colourless bipyramid-shaped crystals of **1** were harvested after a week.

2.2. Single crystal X-ray diffraction

Crystal structure determination by single-crystal X-ray diffraction was performed on an Oxford Diffraction Gemini E Ultra diffractometer using Mo radiation ($\lambda = 0.71073 \text{ \AA}$, operating at 50 kV and 40 mA). Full data sets were collected from 120 to 300 K at intervals of 10 K. Data collection, cell determination and refinement and cell reduction were performed using CrysAlisPro software.⁶ The 120 and 300 K structures were solved using direct methods and successive Fourier difference syntheses, and refined by full matrix least squares procedure on F^2 with anisotropic thermal parameters for all non-hydrogen atoms, using the SHELXTL-PLUS⁷ package of programs *via* the X-Seed interface.⁸ The hydrogen atoms of the formate ligands were located by geometric calculations and refined using a riding mode and isotropic displacement parameters constrained to be 1.2 times those of their adjacent carbon atoms. The hydrogen atoms of the ammonium cations were located via Fourier difference syntheses for both structures, and the disordered ammonium cations in the 300 K structure were treated using a two-fold disorder model. The full crystallographic data and structure refinements at 120 and 300 K are summarized in Table S1. The cell parameters from 120 to 300 K are listed in Table S2.

2.3. Resonant ultrasound spectroscopy (RUS)

The principle of the RUS technique is as follows.⁹ A sample is held lightly between two piezoelectric transducers. The first transducer is driven by a frequency synthesizer at constant amplitude across a range of ultrasonic frequencies (0.1-2 MHz) which in turn causes the sample to resonate at particular frequencies. The second transducer acts as a signal detector which records the response of the sample in terms of its displacements. Peaks in the spectra occur at the frequencies of normal modes of the sample. The resonance frequencies depend on the elastic constants, density, shape and dimensions of the sample. For a sample with high

structure symmetry and regular shape (most commonly a rectangular parallelepiped with faces aligned with crystallographic axes), the elastic constants are determined by solving the inverse problem numerically, and an iteration procedure is used to match the calculated resonance frequencies with the measured spectra. For isotropic materials, there are two independent elastic constants. For single crystals with hexagonal space group, there are five independent elastic constants. The square of a given peak frequency is directly proportional to the elastic constants associated with that normal mode.⁹ RUS measurements were obtained using a single crystal with irregular shape (~0.4 mm, 0.0003 g) in a helium flow cryostat which has been described elsewhere.¹⁰ Data were collected with the sample chamber filled with a few mbar of helium to allow heat exchange between sample and cryostat. The sample was first cooled from 280 K to 10 K with data collection at intervals of 30 K, and then warmed from 10 K to 120 K with intervals of 5 K, and from 120 K to 300 K with intervals of 2 K. 50000 data points were collected for each spectrum in the frequency range from 0.1 to 2.5 MHz. All spectra were transferred to the software package Igor Pro (WaveMetrics) for analysis. Peak positions and the full widths at half maximum (FWHM) of the peaks were determined for a selection of peaks by fitting with an asymmetric Lorentzian function. The mechanical quality factor, Q , was calculated using the relationship $Q = f/\Delta f$, where f is the peak frequency and Δf is the width of the peak at half its maximum height. The inverse of the quality factor, Q^{-1} , is a measure of acoustic dissipation (energy loss) in the sample.

3. Results

3.1. Structural analysis before and after the phase transition

The room temperature structure of framework **1** is in the hexagonal and non-polar space group $P6_322$ with $a_{300\text{K}} = 7.3090(3)$ and $c_{300\text{K}} = 8.1701(3)$ Å, as reported previously.^{5b} Bridging formate ligands connect octahedral Zn(II) ions in an *anti-anti* mode fashion, and

each Zn(II) ion is linked to six neighbouring Zn(II) ions. As a result, the 3D anionic frameworks $[\text{Zn}(\text{HCOO})_3]_n^-$ have a $(4^{12}\cdot 6^3)$ topology with 1D hexagonal channels along the c -axis occupied by NH_4^+ cations (Fig. 1a, b). The NH_4^+ is equally disordered between two positions (coloured in grey and black in Fig. 1a), and hydrogen-bonded to the six HCOO^- ligands in the framework *via* $\text{N}-\text{H}\cdots\text{O}$ bonds with $\text{N}\cdots\text{O}$ distances of 2.971(3) Å and $\text{N}-\text{H}\cdots\text{O}$ angles of 160(1)° (Fig. 1a-b, Table S3). In the low-temperature structure (120 K), the NH_4^+ cation becomes ordered, which changes the hydrogen-bonds between the NH_4^+ and $[\text{Zn}(\text{HCOO})_3]^-$ framework substantially. Specifically, each NH_4^+ in this phase is only hydrogen-bonded to three HCOO^- ligands *via* $\text{N}-\text{H}\cdots\text{O}$ bonds with $\text{N}\cdots\text{O}$ distances of 2.829(3) to 2.866(3) Å and $\text{N}-\text{H}\cdots\text{O}$ angles of 166(2) to 176(2)° (Fig. 1c-d, Table S3). The ordering of the NH_4^+ cations and consequent changes of hydrogen bonding break the symmetry and induce a paraelectric (non-polar, $P6_322$) to ferroelectric (polar, $P6_3$) phase transition. The low temperature phase has cell parameters of $a_{120\text{K}} =$

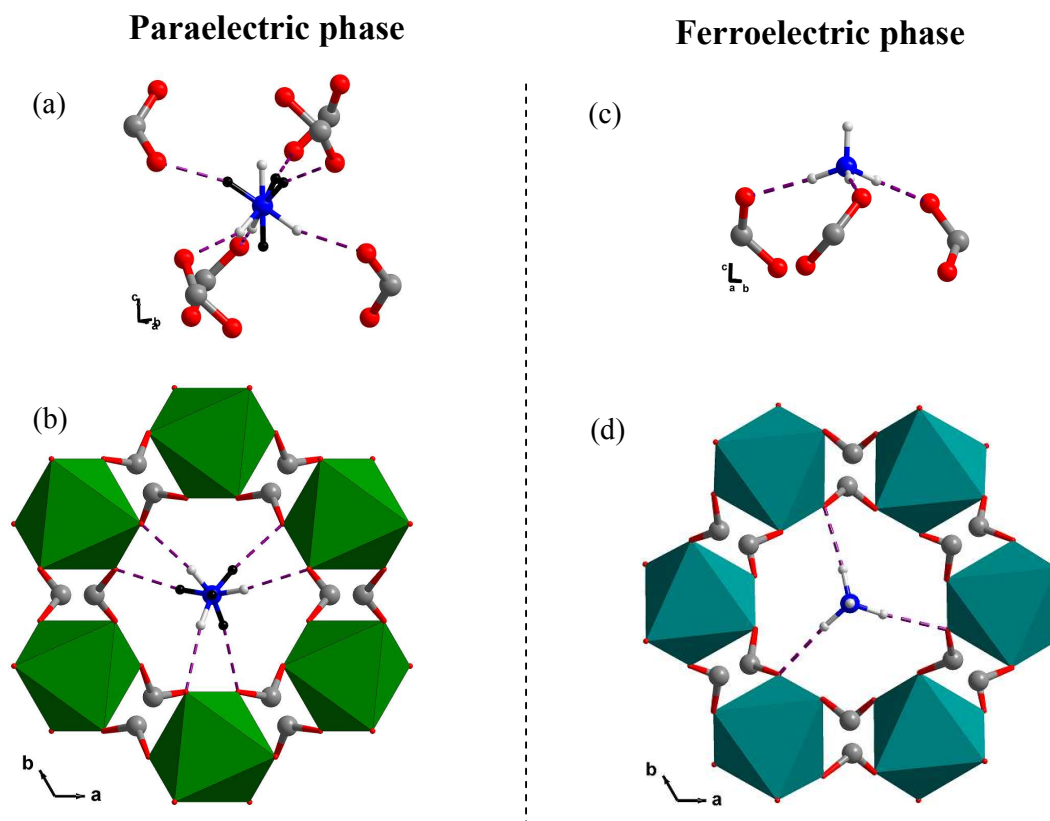


Fig. 1 Crystal structure of framework $[\text{NH}_4][\text{Zn}(\text{HCOO})_3]$, **1**. (a) and (c): the conformations of disordered and ordered NH_4^+ cations in the paraelectric and ferroelectric phases, respectively (the equally disordered ammonium at two positions is illustrated in white and black colours for the paraelectric structure); (b) and (d): paraelectric and ferroelectric structures of framework **1** viewed along the c axis at 300 K and 120 K, respectively. Note: there are three crystallographically independent NH_4^+ cations in the 120 K structure, but the other two are not illustrated in (b) and (d) for clarity. Colour scheme: Zn(II), green or teal; O, red; C, grey; N, blue; H, white and black. N–H...O bonds are represented as dashed purple lines. Hydrogen atoms of formate ligands are omitted for clarity.

12.5946(4) and $c_{120\text{K}} = 8.2087(3)$ Å, corresponding to a unit cell $\sqrt{3}a_{300\text{K}} \times \sqrt{3}a_{300\text{K}} \times c_{300\text{K}}$.^{5b} According to the group-subgroup relations, the low temperature phase is an improper ferroelectric. Variable temperature single-crystal X-ray diffraction (SCXRD) measurements, from 120 to 300 K, show that the para- to ferroelectric phase transition is marked by a nearly continuous and non-linear change in the a -parameter between 180 and 190 K after the low temperature a -parameter has been divided by $\sqrt{3}$ for comparison (Fig. 2). This is consistent with the previous DSC and heat capacity measurements which show an anomaly at ~ 192 K.^{5b}

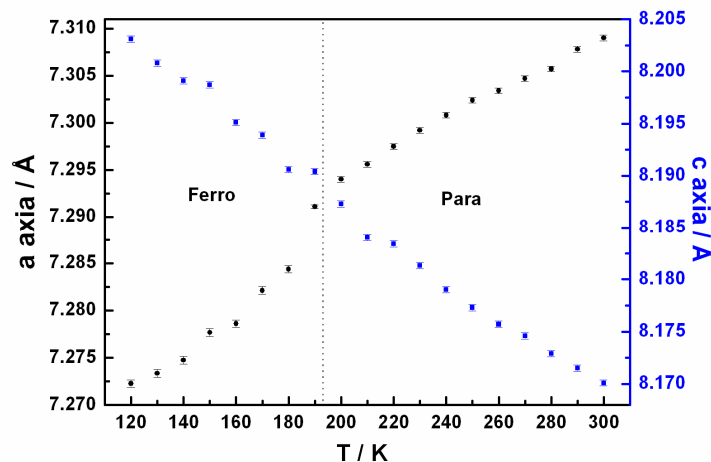


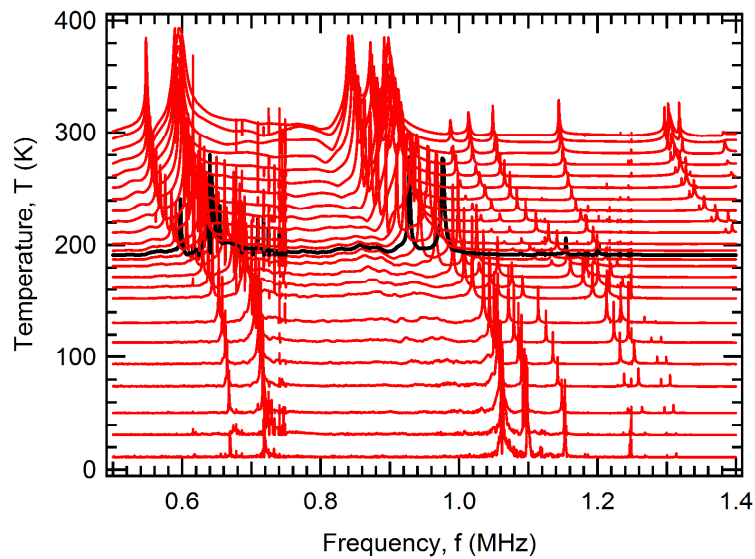
Fig. 2 Lattice parameters of **1** obtained from single-crystal X-ray diffraction at intervals of 10 K from 120 K to 300 K. The dotted line is placed at the transition temperature of 192 K. For comparison, the low temperature a -parameter has been divided by $\sqrt{3}$.

3.2. RUS studies

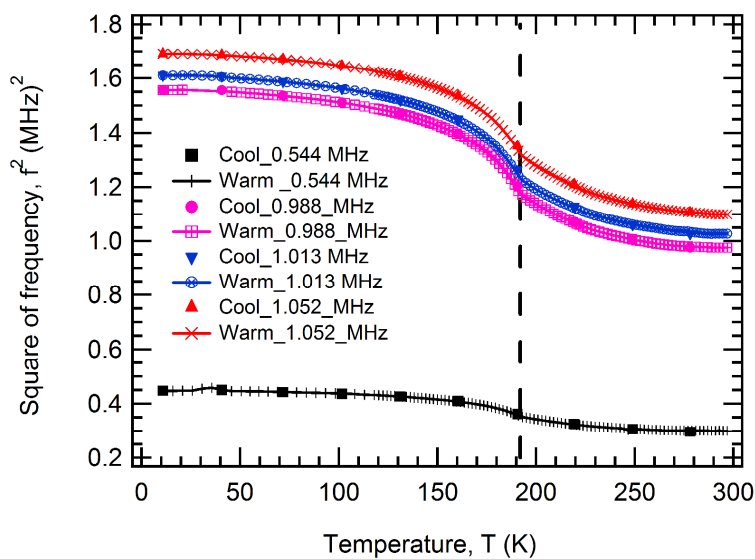
RUS results are shown in Fig. 3 and are internally consistent between cooling and heating. Selected spectra from the single crystal collected during a warming sequence from 10 K to 300 K are illustrated in Fig. 3a and clearly show a change in the trend of peak frequencies near the transition temperature of 192 K. Note that the y -axis is actually amplitude in volts, from the detector transducer, but the spectra have been offset in proportion to the temperature at which they were collected and then axis labeled as temperature.

Data for f^2 and Q^{-1} obtained from fitting selected peaks are shown in Fig. 3b-c. All the resonance peaks have the same form of elastic softening (reducing values of f^2) with increasing temperature, with a marked change in the rate near the expected transition temperature of 192 K (Fig. 3b). With increasing temperature, Q^{-1} gradually increases and also shows anomalies near 192 K. Q^{-1} from the resonance frequency at 0.544 MHz has a peak, and then increases with increasing temperature. Q^{-1} from the resonance frequency near 0.988

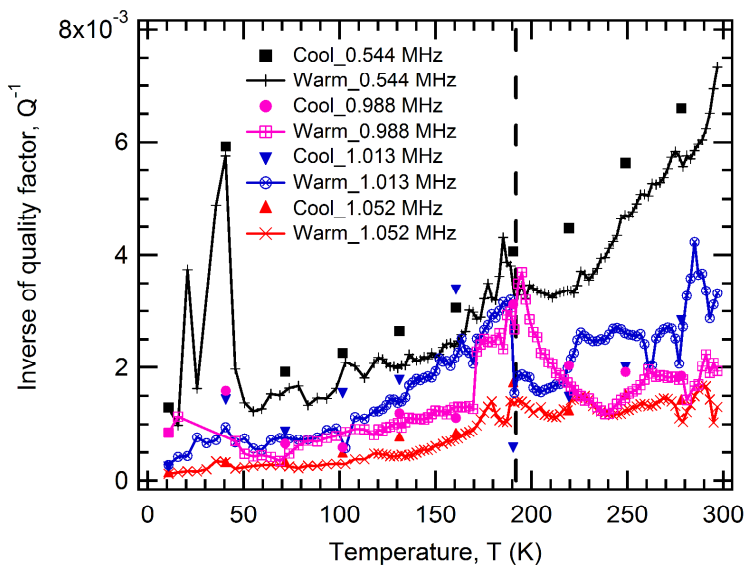
MHz has a peak near 192 K, with lower values below and above this. For the resonance frequency at 1.013 MHz, a step appears near 192 K. Each of these resonances corresponds to a different combination of elastic constants and it seems that the loss pattern differs slightly according to which combination is involved. The apparent anomalies at low temperatures below 50 K for the resonance frequency near 0.544 MHz are due to noise in the data.



(a)



(b)



(c)

Fig. 3 (a) Stack of RUS spectra as a function of frequency for **1** between 10 K and 300 K (the spectrum at 192 K, i.e. the ferroelectric phase transition temperature, is shown in black and other spectra in red). (b) Temperature dependencies of f^2 from fitting of selected resonance peaks. (c) Temperature dependencies of Q^{-1} from fitting of selected resonance peaks. The vertical broken line represents the transition temperature and is shown at 192 K.

4. Discussion

The elastic anomalies and acoustic dissipation near 192 K in $[\text{NH}_4][\text{Zn}(\text{HCOO})_3]$ are closely related to the paraelectric to ferroelectric transition. This is accompanied by the change from the non-polar hexagonal space group $P6_322$ to the polar hexagonal space group $P6_3$, which is triggered by the disorder-order transition of ammonium cations within the structure and the changes of hydrogen bonding.^{5b, 5c} Analogous transitions driven by hydrogen bonding coupled to lattice distortions occur in the mineral lawsonite $[\text{CaAl}_2\text{Si}_2\text{O}_7(\text{OH})_2 \cdot \text{H}_2\text{O}]$,^{10, 11} and these provide the model by which the behaviour of $[\text{NH}_4][\text{Zn}(\text{HCOO})_3]$ can be understood. In lawsonite, changes in hydrogen bonding are accompanied by changes in space

group at ~ 270 and ~ 150 K, and the lowest temperature structure is ferroelectric. It always follows that if there are changes in lattice strain accompanying a phase transition their influence will be seen clearly in changes in the elastic constants.¹² For most displacive transitions, however, the effect of coupling between strain and the driving order parameter is softening of the elastic constants with falling temperature. This is due to the fact that an applied stress would induce a strain, in accordance with Hooke's law, and then, because the strain is coupled with the order parameter there is an additional relaxation of the order parameter. In $[\text{NH}_4][\text{Zn}(\text{HCOO})_3]$ and lawsonite, the trend is of stiffening rather than softening with falling temperature through the transition points, indicating that the order parameter does not relax on the timescale of the measurements. It is therefore probably more appropriate to think of the hydrogen bonding as adding more or less rigid braces to the structure, which cause the elastic stiffening.

In lawsonite, the amount of elastic stiffening due to the transition at transition temperature T_c ~ 270 K, in excess of what would occur if there were no phase transition, scales with the square of the order parameter, q , and is non-linear because the transition is close to tricritical in character, i.e. q^4 is proportional to $(T_c - T)$.¹⁰ The pattern in Fig. 3b is closely similar, though there is also a precursor stiffening effect as the temperature reduces towards ~ 192 K. The paraelectric–ferroelectric transition in $[\text{NH}_4][\text{Zn}(\text{HCOO})_3]$ is also close to tricritical, which is reflected in a continuous and non-linear change in the lattice parameters through the transition temperature (as shown in Fig. 2). A symmetry change from space group $P6_322$ to space group $P6_3$ also occurs in the mineral kaliophilite (KAlSiO_4) and is close to tricritical.¹³

The pattern of acoustic loss in lawsonite involves relatively low values of Q^{-1} below $T_c \sim 270$ K, a peak just below T_c , and then increasing values above T_c .¹⁰ The pattern of acoustic loss in

$[\text{NH}_4][\text{Zn}(\text{HCOO})_3]$ is closely similar, with $T_c \sim 192$ K. The loss mechanism must involve coupling of the hydrogen bonding with local lattice strains but occurring dynamically on a time scale that is not too far from the time scale of mechanical resonances observed by RUS, i.e. $\sim 10^{-6}$ seconds. At $T < T_c$, the relaxation time for hopping of hydrogen atoms between their symmetry related positions in the ordered structure must be substantially longer than this, as reflected also in the elastic stiffening behaviour. As T is approaching T_c from both above and below the relaxation time tends to towards $\sim 10^{-6}$ seconds since there is a marked peak in the acoustic loss. At $T > T_c$, the loss mechanism is presumably then related to dynamical disordering both of the hydrogen positions and of lattice distortions in the fully disordered structure.

5. Conclusions

RUS studies of $[\text{NH}_4][\text{Zn}(\text{HCOO})_3]$ have shown elastic anomalies and acoustic dissipation near 192 K, which are induced by the ferroelectric transition triggered by the disorder-order transition of ammonium cations within the structure and the changes of hydrogen bonding. Increases in the elastic constants below the transition point indicate that hydrogen bonds act as braces, giving more rigidity to the structure, in contrast with displacive phase transitions which typically give rise to softening. Dynamical disordering of the hydrogen positions and coupling with the lattice strain is responsible for significant acoustic loss, which is greater above the transition point than below.

Acknowledgements

This work was supported by the Fundamental Research Funds for the Central Universities (WUT: 143101002), European Research Council (ERC) funding, and grants from the Natural

Environment Research Council (NERC) under grant numbers NE/B505738/1 and NE/F017081/1.

Notes and references

- 1 (a) A. K. Cheetham and C. N. R. Rao, *Science*, 2007, **318**, 58; (b) C. N. R. Rao, A. K. Cheetham and A. Thirumurugan, *J. Phys.: Condens. Matter*, 2008, **20**, 083202; (c) J. R. Long and O. M. Yaghi, *Chem. Soc. Rev.*, 2009, **38**, 1213; (d) M. Kurmoo, *Chem. Soc. Rev.*, 2009, **38**, 1353; (e) W. Zhang and R.-G. Xiong, *Chem. Rev.*, 2012, **112**, 1163.
- 2 (a) P. Jain, V. Ramachandran, R. J. Clark, H. D. Zhou, B. H. Toby, N. S. Dalal, H. W. Kroto and A. K. Cheetham. *J. Am. Chem. Soc.*, 2009, **131**, 13625; (b) G. C. Xu, W. Zhang, X. M. Ma, Y. H. Chen, L. Zhang, H. L. Cai, Z. M. Wang, R. G. Xiong, S. Gao., *J. Am. Chem. Soc.*, 2011, **133**, 14948; (c) A. Stroppa, P. Jain, M. Marsman, J. M. Perez-Mato, A. K. Cheetham, H. W. Kroto and S. Picozzi, *Angew. Chem. Int. Ed.*, 2011, **50**, 5847; (d) A. Stroppa, P. Barone, P. Jain, J. M. Perez-Mato and S. Picozzi, *Adv. Mater.*, 2013, **25**, 2284; (e) D. D. Sante, A. Stroppa, P. Jain and S. Picozzi, *J. Am. Chem. Soc.*, 2013, **135**, 18216. (f) L. Cañadillas-Delgado, O. Fabelo, J. A. Rodriguez-Velamazán, M.-H. Lemée-Cailleau, S. A. Mason, E. Pardo, F. Lloret, J.-P. Zhao, X.-H. Bu, V. Simonet, C. V. Colin, and J. Rodriguez-Carvajal *J. Am. Chem. Soc.*, 2012, **134**, 19772; (g) M. Maćzka, A. Ciupa, A. Gaĝor, A. Sieradzki, A. Pikul, B. Macalik and M. Drozd, *Inorg. Chem.*, 2014, **53**, 5260; (h) J. Han, S. Nishihara, K. Inoue and M. Kurmoo, *Inorg. Chem.*, 2014, **53**, 2068.
- 3 (a) J. C. Tan, C. A. Merrill, J. B. Orton and A. K. Cheetham, *Acta. Mater.*, 2009, **57**, 3481; (b) J. C. Tan, T. D. Bennett and A. K. Cheetham, *Proc. Natl. Acad. Sci. USA*, 2010, **107**, 9938; (c) J. C. Tan and A. K. Cheetham, *Chem. Soc. Rev.*, 2011, **40**, 1059; (d) J. C. Tan, B. Civalieri, C. C. Lin, L. Valenzano, R. Galvelis, P. F. Chen, T. D. Bennett, C. Mellot-

- Draznieks, C. M. Zicovich-Wilson and A. K. Cheetham, *Phys. Rev. Lett.*, 2012, **108**, 095502; (e) R. I. Thomson, P. Jain, A. K. Cheetham, J. M. Rawson and M. A. Carpenter, *Phys. Rev. B*, 2012, **86**, 214304; (f) W. Li, Z. Zhang, E. G. Bithell, A. S. Batsanov, P. T. Barton, P. J. Saines, P. Jain, C. J. Howard, M. A. Carpenter and A. K. Cheetham, *Acta Mater.*, 2013, **61**, 4928; (g) W. Li, A. Thirumurugan, P. T. Barton, Z. Lin, S. Henke, H. H.-M. Yeung, M. T. Wharmby, E. G. Bithell, C. J. Howard and A. K. Cheetham, *J. Am. Chem. Soc.*, 2014, **136**, 7801; (h) M. Mączka, M. Ptak and S. Kojima, *Appl. Phys. Lett.*, 2014, **104**, 222903.
- 4 (a) X. Y. Wang, L. Gan, S. W. Zhang and S. Gao, *Inorg. Chem.*, 2004, **43**, 4615; (b) P. Jain, N. S. Dalal, B. H. Toby, H. W. Kroto, and A. K. Cheetham, *J. Am. Chem. Soc.*, 2008, **130**, 10450; (c) J. C. Tan, P. Jain and A. K. Cheetham, *Dalton Trans.*, 2012, 41, 3949; (d) M. Mączka, M. Ptak and L. Macalik, *Vib. Spectrosc.*, 2014, **71**, 98.
- 5 (a) Z. M. Wang, B. Zhang, K. Inoue, H. Fujiwara, T. Otsuka, H. Kobayashi and M. Kurmoo, *Inorg. Chem.*, 2007, **46**, 437; (b) G. C. Xu, X. M. Ma, L. Zhang, Z. M. Wang, and S. Gao, *J. Am. Chem. Soc.*, 2010, **132**, 9588; (c) G. C. Xu, W. Zhang, X. M. Ma, Y. H. Chen, L. Zhang, H. L. Cai, Z.M. Wang, R. G. Xiong and S. J. Gao, *J. Am. Chem. Soc.*, 2011, **133**, 14948; (d) R. Shang, G. Xu, Z. Wang and S. Gao, *Chem. Eur. J.*, 2014, **20**, 1146; (e) M. Mączka, A. Pietraszko, B. Macalik and K. Hermanowicz, *Inorg. Chem.*, 2014, **53**, 787.
- 6 *CrysAlis^{Pro}*, Oxford Diffraction Ltd., Version 1.171.36.32.
- 7 G. M. Sheldrick, *Acta Crystallogr. Sect. A*, 2008, **64**, 112.
- 8 L. J. Barbour, *J. Supramol. Chem.*, 2001, **1**, 189.
- 9 (a) A. Migliori, J. L. Sarrao, W. M. Visscher, T. M. Bell, M. Lei, Z. Fisk and R. G. Leisure, *Physica B*, 1993, **183**, 1; (b) A. Migilori and J. L. Sarraro, *Resonant ultrasound*

spectroscopy: applications to physics, Material measurements and non-destructive evaluation. New York: Wiley, 1997.

- 10 R. E. A. McKnight, M. A. Carpenter, T. W. Darling, P. A. Taylor. *Am. Mineral.*, 2007, **92**, 1665.
- 11 (a) E. Libowitzky and T. Armbruster, *Am. Mineral.*, 1995, **80**, 1277; (b) E. Libowitzky and G. R. Rossman, *Am. Mineral.*, 1996, **81**, 1080; (c) P. Sondergeld, W. Schranz, A. V. Kityk, M. A. Carpenter and E. Libowitzky, *Phase Transitions*, 2000, **71**, 189; (d) P. Sondergeld, W. Schranz, A. Troster, M. A. Carpenter, E. Libowitzky and A. V. Kityk, *Phys. Rev. B*, 2000, **62**, 6143; (e) P. Sondergeld, W. Schranz, A. Troster, H. Kabelka, H. W. Meyer, M. A. Carpenter, Z. Lodziana and A. V. Kityk, *Phys. Rev. B*, 2001, **64**, 024105; (f) H. W. Meyer, M. A. Carpenter, A. Graeme-Barber, P. Sondergeld and W. Schranz, *Eur. J. Mineral.*, 2000, **12**, 1139; (g) H. W. Meyer, S. Marion, P. Sondergeld, M. A. Carpenter, K. S. Knight, S. A. T. Redfern and M. T. Dove, *Am. Mineral.*, 2001, **86**, 566; (h) J. M. Martin-Olalla, S. A. Hayward, H. W. Meyer, S. Ramos, J. del Cerro and M. A. Carpenter, *Eur. J. Mineral.*, 2001, **13**, 5; (i) M. A. Carpenter, H. W. Meyer, P. Sondergeld, S. Marion and K. S. Knight, *Am. Mineral.*, 2003, **88**, 534; (j) M. A. Carpenter, *Am. Mineral.*, 2006, **91**, 229.
- 12 (a) W. Rehwald, *Adv. in Phys.*, 1973, **22**, 721; (b) B. Lüthi and W. Rehwald, *Topics in Current Physics*, 1981, **23**, 131; (c) M. A. Carpenter and E. K. H. Salje, *Eur. J. Mineral.*, 1998, **10**, 693.
- 13 D. Cellai, M. A. Carpenter and P. J. Heaney, *Eur. J. Mineral.*, 1992, **4**, 1209.